Effects of winds on the leftover hydrogen in massive stars following Roche lobe overflow

Avishai Gilkis [ID],[1]★ Jorick S. Vink,[2]★ J. J. Eldridge [ID][3]★ and Christopher A. Tout [ID][1]

[1]*Institute of Astronomy, University of Cambridge, Madingley Road, Cambridge CB3 0HA, UK*
[2]*Armagh Observatory and Planetarium, College Hill, Armagh BT61 9DG, UK*
[3]*Department of Physics, University of Auckland, Private Bag 92019, Auckland 1010, New Zealand*

ABSTRACT

We find that applying a theoretical wind mass-loss rate from Monte Carlo radiative transfer models for hydrogen-deficient stars results in significantly more leftover hydrogen following stable mass transfer through Roche lobe overflow than when we use an extrapolation of an empirical fit for Galactic Wolf-Rayet stars, for which a negligible amount of hydrogen remains in a large set of binary stellar evolution computations. These findings have implications for modelling progenitors of Types Ib and IIb supernovae. Most importantly, our study stresses the sensitivity of the stellar evolution models to the assumed mass-loss rates and the need to develop a better theoretical understanding of stellar winds.

Key words: binaries: close – stars: evolution – stars: massive – stars: mass-loss – supernovae: general – stars: winds, outflows.

1 INTRODUCTION

A large fraction of massive stars, if not all of them, end their lives as energetic and luminous supernovae (SNe). These core-collapse SNe (CCSNe) are classified according to their observed light curves and spectral features. One of the most conspicuous characteristics for CCSN classification is the presence of hydrogen spectral lines (Filippenko 1997). Type II SNe are those for which hydrogen is observed, while hydrogen is absent in spectra of Type I SNe (specifically Ib and Ic, for massive stars). A special case of Type II SNe, for which hydrogen spectral features are observed at early stages but later disappear, is termed IIb (e.g. SN 1993J; Nomoto et al. 1993).

Dessart et al. (2011) find, in their modelling, that a total hydrogen mass in the stellar envelope of $M_H \gtrsim 0.001 \, M_\odot$ results in a Type IIb SN rather than a Type Ib. Types Ib and IIb CCSNe are thought to arise from similar evolutionary channels which result in a small amount of hydrogen left in the stellar envelope (Yoon, Dessart & Clocchiatti 2017). Recent studies give priority to binary evolution channels for progenitors of both Type Ib (Yoon 2015) and Type IIb (e.g. Podsiadlowski et al. 1993; Claeys et al. 2011; Soker 2017), though single-star progenitors are not ruled out (Kotak & Vink 2006; Yoon et al. 2012). It is noteworthy that the remnant Cassiopeia A, which is agreed to have been a Type IIb, contains no remaining companion star (Kochanek 2018; Kerzendorf et al. 2019).

The basic scenario for Types Ib and IIb SNe in binary systems (Yoon et al. 2017) is that the primary star expands as it evolves until it fills its Roche lobe, when mass transfer starts owing to Roche lobe overflow (RLOF). If the mass transfer is stable, it continues until a small amount of hydrogen is left in the envelope of the primary, at which point the star starts to shrink. Further mass-loss is through stellar winds.[1] The amount of hydrogen left, if any, depends on the assumed mass-loss rate at this stage. Here we aim to emphasize the importance of the post-RLOF stellar winds, and the associated uncertainties, for the properties of stellar model envelopes and the leftover hydrogen in them.

2 METHOD

We use the Modules for Experiments in Stellar Astrophysics code (MESA, version 10398, Paxton et al. 2011, 2013, 2015, 2018) to evolve binary stars with a metallicity of $Z = 0.019$ from the main sequence until the end of carbon burning in the core of the primary. This stage is just years before iron core collapse and the properties of the outer parts of the star are not expected to change (Woosley et al. 2002). We ran models with initial primary masses of $M_1/M_\odot \in \{12, 14, 16, 19, 22, 25\}$, secondary masses listed in Table 1, and orbital periods of $P_i/d \in \{5, 10, 18, 33, 60, 110, 201, 367, 669, 1219, 2223\}$. Effects related to rotation, such as rotational mixing and tidal synchronization, are not taken into account. This choice was made to concentrate on the effect under study in a

---

★ E-mail: agilkis@ast.cam.ac.uk (AG); jorick.vink@armagh.ac.uk (JSV); j.eldridge@auckland.ac.nz (JJE)

[1] Additional RLOF episodes can occur, for certain initial parameters, when the primary expands again.

Table 1. Initial masses for stellar evolution calculations.

$M_1/M_\odot$	$0.9 > q > 0.8$ $M_2/M_\odot$	$0.7 > q > 0.6$ $M_2/M_\odot$	$0.45 > q > 0.35$ $M_2/M_\odot$
12	10	8	5
14	12	9	5
16	14	10	6
19	16	12	7
22	19	14	8
25	22	16	9

simple manner. The following sub-sections detail the main aspects of the stellar modelling and additional technical details on code implementations are in Appendix A.

2.1 Wind mass-loss

Mass-loss through winds is according to Vink, de Koter & Lamers (2001) for hydrogen-rich hot stars and according to de Jager, Nieuwenhuijzen & van der Hucht (1988) for effective surface temperatures below 10^4 K. For hot stars with hydrogen surface abundances X_s below 0.4, we use one of two different mass-loss prescriptions, either that of Vink (2017) or Nugis & Lamers (2000). The mass-loss rate of Vink (2017), which we herein refer to as V17, is

$$\log_{10}\left(\dot{M}/M_\odot\,\mathrm{yr}^{-1}\right) = -13.3 + 1.36\log_{10}\left(L/L_\odot\right)$$
$$+ 0.61\log_{10}\left(Z_s/0.019\right), \qquad (1)$$

where $\dot{M}$ is the mass-loss rate, L is the stellar luminosity, and Z_s is the metallicity at the photosphere. The mass-loss prescription following Nugis & Lamers (2000), herein NL00, is

$$\log_{10}\left(\dot{M}/M_\odot\,\mathrm{yr}^{-1}\right) = -11.0 + 1.29\log_{10}\left(L/L_\odot\right)$$
$$+ 1.7\log_{10}\left(Y_s\right) + 0.5\log_{10}\left(Z_s\right), \qquad (2)$$

where Y_s is the surface helium abundance. We note that the V17 prescription has no dependence on Y_s because this is considered to be unrelated to the physics of the wind driving.

The NL00 recipe is based on empirical modelling of observed Wolf-Rayet (WR) stars. Unfortunately only a few stripped stars are known so we cannot rely on empirical rates for lower mass stripped helium stars as we can for classical WR stars.[2] The one exception could be HD45166 (Groh, Oliveira & Steiner 2008) but this system might have undergone a different evolution from the simple RLOF we model here. There are too few actual measured mass-loss rates for stripped stars (Yoon 2015) to derive a reliable empirical mass-loss rate prescription for helium stars with masses and luminosities lower than those of the classical WR stars. One option to overcome this observational inadequacy is to extrapolate the NL00 recipe towards the regime of lower masses and lower luminosities but the dependencies on helium abundance Y_s and total metallicity Z_s in NL00 are thought to be unphysical (e.g. Puls, Vink & Najarro 2008). Extrapolation of the NL00 recipe to a parameter regime for which it was not derived is then of rather limited value.

Vink (2017) makes a pilot study that provides theoretical predictions for stripped helium stars using Monte Carlo models with a fixed effective temperature of 50 000 K. These winds remain

[2]The NL00 prescription has some difficulties with classical WR stars as well (Yoon 2017).

optically thin in the simulated parameter range and it remains to be seen whether the winds become optically thicker at higher effective temperatures. A higher effective temperature T_{eff} would imply a smaller star which is more likely to become optically thick so that the mass-loss rate might increase substantially. If the winds were to remain optically thin at higher T_{eff}, we would not expect the mass-loss rate to change dramatically unless there is insufficient line opacity at higher T_{eff} or there is an opacity or bistability jump, as found for hydrogen-rich stars at lower T_{eff} (Vink, de Koter & Lamers 1999).

In any case a transition between optically thin stripped helium stars and optically thick WR stars might be expected somewhere in the helium star regime, similar to the mass-loss kink in the hydrogen-rich part of the Hertzsprung–Russell diagram (Vink et al. 2011; Bestenlehner et al. 2014). Although more work is needed to cover the entire parameter space and to investigate and scrutinize the accuracy of the Vink (2017) pilot study, we consider the order-of-magnitude lower mass-loss rates provided by this theoretical scheme compared to the simple extrapolations of NL00 to lower masses and luminosities of stripped stars to be more likely correct.

2.2 Mass transfer by Roche lobe overflow

The mass-transfer rate by RLOF $\dot{M}_{\mathrm{tr}}$ is calculated according to the scheme of Kolb & Ritter (1990). We implement an updated mass-transfer scheme[3] so that the mass-transfer efficiency is limited by the thermal time-scale of the accretor,

$$\beta\dot{M}_{\mathrm{tr}} \leq M/\tau_{\mathrm{th}}, \qquad (3)$$

where β is the mass transfer efficiency and the thermal time-scale is defined by

$$\tau_{\mathrm{th}} \equiv \frac{GM^2}{LR}, \qquad (4)$$

with R and M the photospheric radius and mass of the primary. In addition, our mass transfer efficiency smoothly drops to zero if the radius of the secondary enters the range $0.99 < R_2/R_{\mathrm{L},2} < 1.0$, where R_2 is the photospheric radius of the secondary and $R_{\mathrm{L},2}$ is its Roche lobe radius.[4] Otherwise the mass transfer efficiency is 0.9, though in theory it might also be reduced owing to the spin-up of the secondary (Packet 1981). Tidal synchronization also affects the orbital evolution in close systems. Our modelling assumptions were chosen to allow for a large range of initial and final conditions to be investigated. For the current purpose of demonstrating the effect of stellar winds, this is sufficient.

2.3 Orbital angular momentum

The orbital separation evolves as angular momentum is lost from the system, affecting the widening of the system and so the occurrence of late mass-transfer episodes. Material lost from the primary in a wind carries away the specific angular momentum of the orbit of the primary. The stellar wind of the secondary also leads to angular momentum loss but less so. Material lost from the system because of inefficient mass transfer, as described in Section 2.2 and

[3]See Appendix A for details.
[4]This is usually avoided by following equation (3) but not in all cases. These limitations on the mass accretion arise because the material is not tightly bound by the gravity of the secondary and so is assumed to be lost from the system.
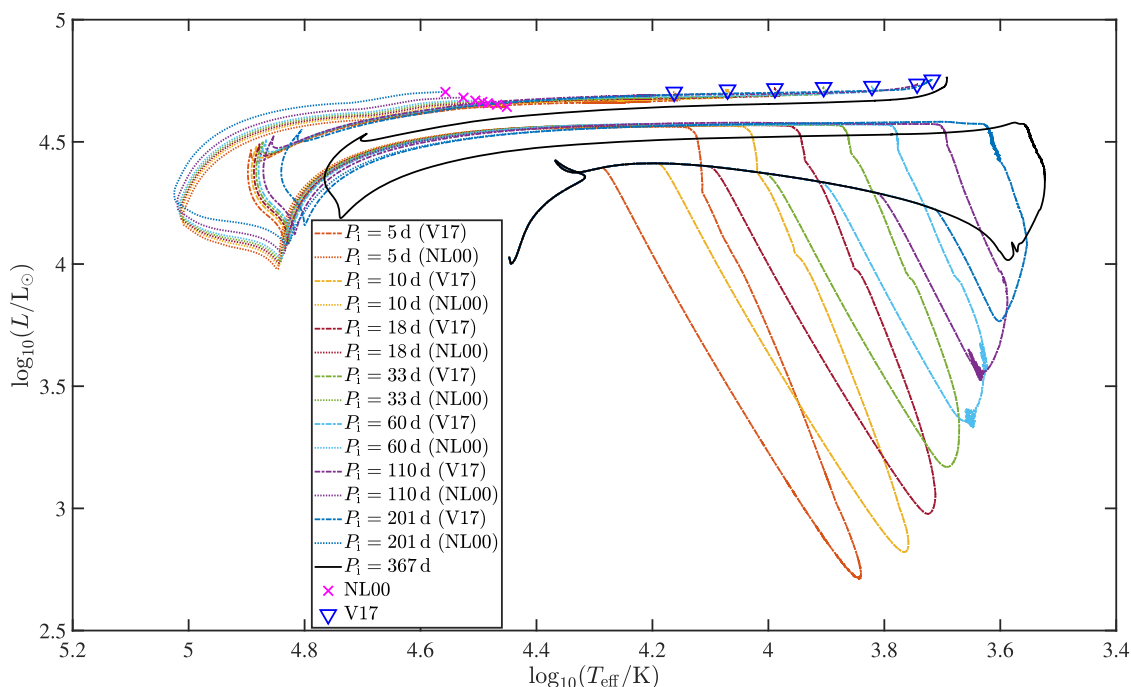
Figure 1. Evolutionary tracks on the Hertzsprung–Russell diagram for models with a primary mass of $M_1 = 12\,M_\odot$ and a secondary initial mass of $M_2 = 10\,M_\odot$ with the initial orbital periods and mass-loss prescriptions indicated in the inset. For initial periods of 201 d and shorter, two different mass-loss rates were used after the surface hydrogen abundance dropped below 0.4. The evolutionary end points are marked with triangles for the V17 models and crosses for the NL00 models.

Appendix A, carries away the specific angular momentum of the secondary.

2.4 Mixing

The Ledoux criterion is applied to define convective regions, in which mixing is according to a mixing-length theory (Henyey, Vardya & Bodenheimer 1965), with $\alpha_{MLT} = 1.5$. Semiconvection is according to Langer, Fricke & Sugimoto (1983), with an efficiency parameter of $\alpha_{sc} = 1.0$. Overshooting above convective regions is as by Herwig (2000). We include thermohaline mixing by the method of Kippenhahn, Ruschenplatt & Thomas (1980).

The dependence of our results on the initial parameters quantitatively changes for different assumptions for the mixing processes. Sukhbold, Woosley & Heger (2018) find that the time a stellar model spends as a blue supergiant relative to the time it spends as a red supergiant depends on semiconvection so we might expect that, with less efficient semiconvective mixing, stellar models would reach large radii at earlier times, changing the dependence of our results on the initial periods. Augmented overshooting increases the helium core masses. Rotational mixing, which we do not account for, can similarly affect our results. The various mixing processes, as well as the definitions of convective boundaries, can affect the stellar mass-loss rate through the composition dependence in equation (2).

3 RESULTS

Fig. 1 shows several example evolutionary tracks on a Hertzsprung–Russell diagram for an initial primary mass of $M_1 = 12\,M_\odot$ and a secondary initial mass of $M_2 = 10\,M_\odot$, several initial orbital periods between 5 and 367 d and the different mass-loss schemes for hydrogen-deficient stars discussed in Section 2.1. For initial periods

of $P_i \geq 367$ d the surface hydrogen abundance remained above 0.4 throughout the evolution. For $P_i < 367$ d the evolutionary tracks diverge after the surface hydrogen abundance drops below 0.4: models with the NL00 mass-loss rate end with significantly higher effective surface temperatures. The V17 models are cooler and have larger photospheric radii owing to a small but non-negligible amount of hydrogen left in their envelopes, as discussed below. The V17 models with $P_i \leq 33$ d in Fig. 1 experience a second phase of mass transfer after filling their Roche lobes as helium giants. The V17 models with $60 \leq P_i/d \leq 201$ in Fig. 1 are close to filling their Roche lobes. Whether a second phase of mass transfer commences depends on the initial masses and can occur also for initial periods longer than 60 d (see Appendix B). Hereinafter all models discussed and presented are those for which the surface hydrogen abundance drops below 0.4 during the evolution so that the NL00 and V17 mass-loss prescriptions are switched on. Models with similar characteristics might also result when $X_s > 0.4$.

Fig. 2 shows the final effective surface temperature for all the models which reached carbon depletion with $X_s < 0.4$ as a function of the total leftover hydrogen mass M_H. Almost all models with the NL00 mass-loss rate ended up with virtually no hydrogen left at all, while the models for which the V17 mass-loss rate was used all have $M_H > 0.0008\,M_\odot$ and most have $M_H > 0.01\,M_\odot$ at the end. This is because the V17 prescription results in post-RLOF mass-loss rates about an order of magnitude lower than the NL00 prescription.

There are several apparent trends in Fig. 2. The sequence for lower temperatures is for models with final masses in the range $2.95 < M/M_\odot < 3.41$ (helium core masses of $2.92 < M_c/M_\odot < 3.25$), the mid-temperature sequence is for models with final masses in the range $3.75 < M/M_\odot < 4.3$ (helium core masses of $3.69 < M_c/M_\odot < 4.12$) and the sequence at the top is for the higher mass models with $4.74 < M/M_\odot$ (helium core masses of $4.6 < M_c/M_\odot$).
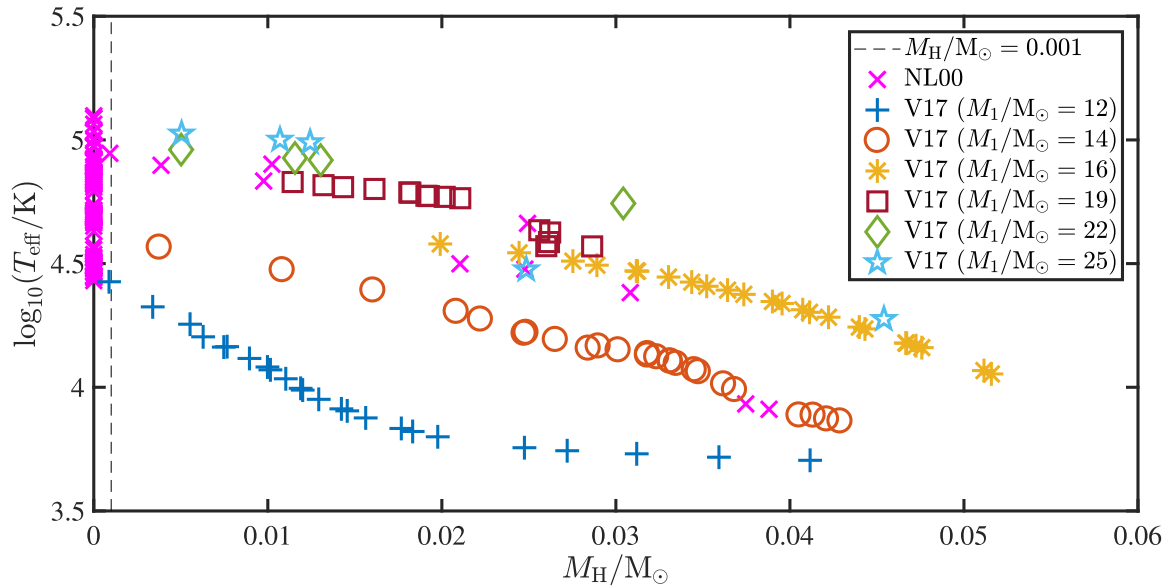
Figure 2. Effective surface temperature $T_{\rm eff}$ as function of total hydrogen mass $M_{\rm H}$ in the final stellar models for which the surface hydrogen abundance is less than 0.4. The initial mass of the primary is indicated for the V17 models. The vertical dashed line indicates the threshold of $M_{\rm H} \gtrsim 0.001\,{\rm M_\odot}$ for Type IIb SNe (Dessart et al. 2011).

This is because more massive helium cores are hotter, while an extended envelope above them reduces the effective photospheric temperature.

Fig. 3 shows how the luminosity of the final models varies with their effective surface temperature. The NL00 models mostly follow a well-defined sequence, similar to that reported by others (e.g. Yoon et al. 2017). The V17 models group into several sequences according to their mass. Observational properties of Type IIb progenitors are plotted, with the hotter falling near our V17 models while the cooler probably have slightly more hydrogen in their envelopes.

Fig. 4 shows the photospheric radii of the final models as a function of the final stellar mass. The NL00 models mostly follow an inverse mass–radius relation, as has been reported for evolved helium stars (e.g. Habets 1986; Yoon et al. 2017). The V17 models tend to become much more expanded because of their hydrogen envelopes. The sequences of V17 models with a narrow mass range and large range in radii correspond to the trends seen in Fig. 2 and discussed above. All models follow very closely the same mass–luminosity relation, $\log_{10}(L/L_\odot) \simeq 1.6 \log_{10}(M/M_\odot) + 3.9$ for $3 \lesssim M/M_\odot \lesssim 8$, because the small additional mass of hydrogen does not contribute to the output luminosity.

Fig. 5 shows the absolute narrow-band visual magnitude M_v of the final models estimated, as by Yoon et al. (2012), with a bolometric correction of ${\rm BC} = 22.053 - 5.306 \log_{10}(T_{\rm eff}/{\rm K})$ for $T_{\rm eff} > 14\,330\,{\rm K}$ and ${\rm BC} = 0$ for $T_{\rm eff} \leq 14\,330\,{\rm K}$. This is a rudimentary approximation and is not based on detailed atmosphere models (e.g. Eldridge et al. 2017). However, it is sufficient to indicate that less radiation is emitted in the narrow visual-band for the hotter models, because almost all the NL00 models have visual magnitudes fainter than -5, while the V17 models are mostly brighter. The lower mass models tend to be even brighter than the WR stars, in terms of M_v, prior to explosion. In some cases, though these are the minority, the secondary is brighter than the primary. These are mostly stars which overflow their Roche lobe again after a late expansion phase. There are more such cases for the

V17 models that expand significantly more than the NL00 models (Fig. 4).

Further mass transfer by RLOF after the simulation ends is not expected to change the properties of the models as CCSN progenitors vary much because the few years until core collapse do not allow for a significant change in the envelope mass, even when it is already quite small. However, some models are already affected by a late mass-transfer phase that begins long before core carbon depletion and is included in the simulation. This has the effect, for example, of limiting the photosphere size to the Roche lobe radius. To assess the importance of this effect, we evolved the same stars from core helium depletion without companions. The results of these additional runs show that individual cases then expand more and have cooler effective temperatures, most notably the systems with initial primary masses of $M_1 = 12$ and $14\,{\rm M_\odot}$ for which the radius can be an order of magnitude larger and the temperature a factor of 2 lower, but the overall range of stellar properties, such as temperatures and radii, are unchanged. The total mass of hydrogen left in the envelope is affected by the late mass-transfer phase because mass is lost through RLOF as well as by stellar winds. The minimal hydrogen mass for the V17 models, evolved as single stars after core helium depletion, is $0.005\,{\rm M_\odot}$, somewhat greater than the $0.0008\,{\rm M_\odot}$ for the models that include the late mass-transfer phase (Fig. 2). For those with initial masses of $M_1 = 12$ and $14\,{\rm M_\odot}$, $M_{\rm H} > 0.018\,{\rm M_\odot}$. These modest quantitative differences do not substantially affect our main conclusions.

The mass-transfer rates for models that experience late RLOF are typically $\dot{M} \approx 10^{-5} \times {\rm M_\odot\,yr^{-1}}$. This is an order-of-magnitude lower than the rates of about $10^{-4} \times {\rm M_\odot\,yr^{-1}}$ given by Tauris et al. (2015) because they have mass transfer from a helium star on to a less massive neutron star, while in our models the late mass transfer is always from a hydrogen-poor star on to a more massive companion, because the earlier mass-transfer episode
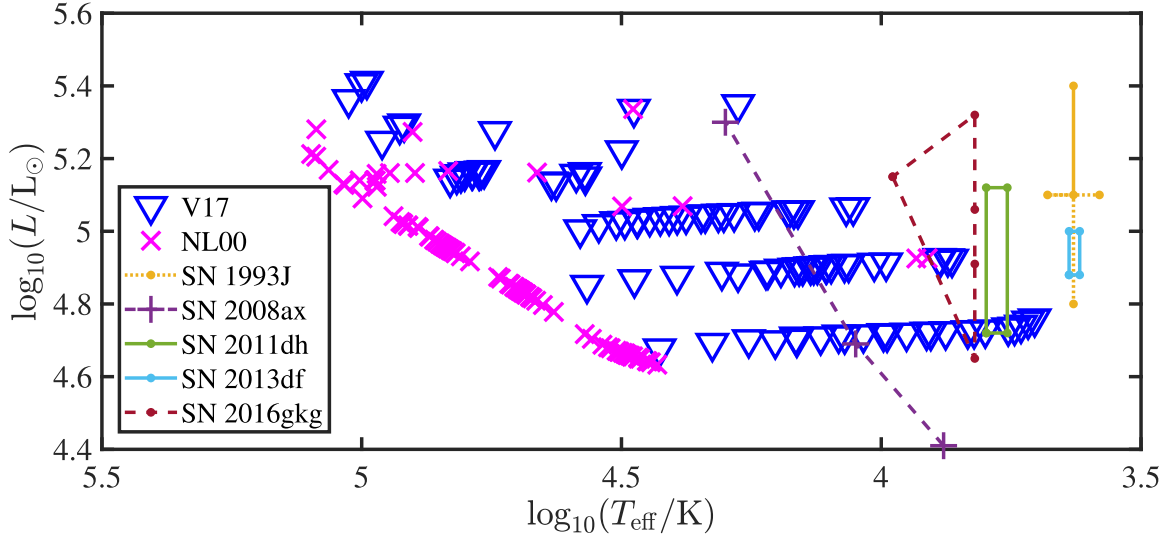
Figure 3. Luminosity as function of effective surface temperature for all models with $X_s < 0.4$. Also plotted are progenitors of Type IIb SNe, SN 1993J (Maund et al. 2004), SN 2008ax (Folatelli et al. 2015), SN 2011dh (Maund et al. 2011), SN 2013df (Van Dyk et al. 2014), and SN 2016gkg (Kilpatrick et al. 2017 for the hotter estimate; Tartaglia et al. 2017 for the cooler points; see also Arcavi et al. 2017).
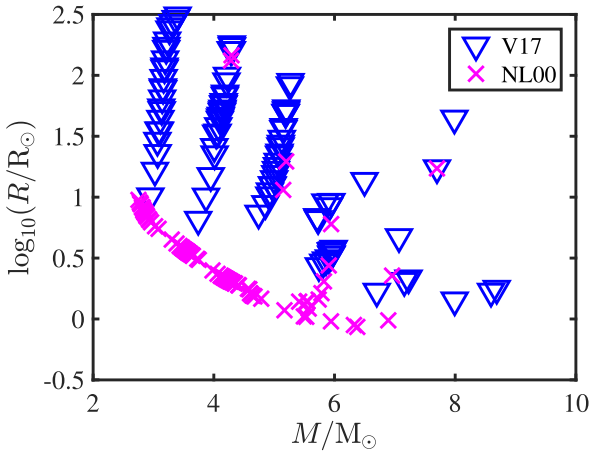
Figure 4. Photospheric radius as function of final mass for all models with $X_s < 0.4$.
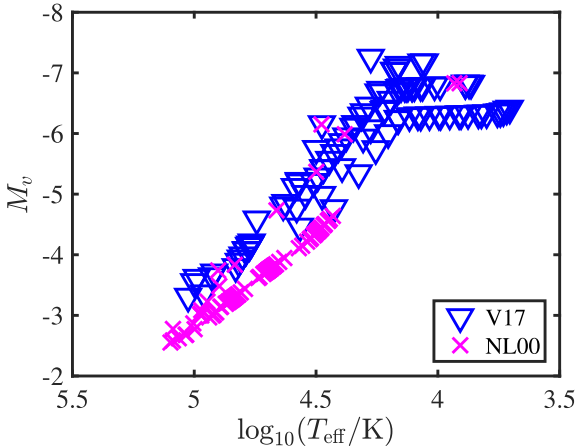
Figure 5. Absolute narrow-band visual magnitude M_v as a function of effective surface temperature for all models with $X_s < 0.4$.

inverted the mass ratio.[5] Further details for all our models are given in Appendix B.

4 SUMMARY AND DISCUSSION

We find that the retention of hydrogen, in the primary of a massive binary system, is highly sensitive to the assumed stellar wind mass-loss rate after RLOF. The two different mass-loss rates used in our study (Nugis & Lamers 2000 and Vink 2017) give rise to potential CCSN progenitors with very different characteristics. Almost all models that employed the NL00 winds lost all of their hydrogen, while models with the V17 mass-loss prescription did not. These results are of course metallicity-dependent because mass-loss by line-driven winds depends on the chemical abundances in the photosphere, as is evident from the dependence on Z_s in equations (1) and (2).

The evolutionary endpoints of the V17 models also tended towards lower temperatures, larger photospheric radii, and to surface helium abundances covering a wide range up to about 0.9. The NL00 models almost all have a helium surface abundance of $Y_s \gtrsim 0.98$ because no hydrogen is left. Acknowledging the uncertainties in modelling SNe spectra and light curves, we can cautiously say that use of the V17 mass-loss rate instead of the NL00 shifts binary progenitor models for CCSNe over a large initial parameter space from Type Ib to Type IIb. For lower metallicites the mass-loss rate is expected to be smaller so there would be even more SNe of Type IIb relative to SNe of Type Ib, as pointed out by Yoon et al. (2017).

The V17 models in our study are mostly brighter in the visual than our NL00 models (Fig. 5). It would also be hard to reconcile the V17 models, which are mostly quite visually bright (low M_v), with the detection limits of Type Ib SNe (Eldridge et al. 2013; McClelland & Eldridge 2016). It is likely that stripped stars have lower wind mass-loss rates than given by NL00 and, with our experiment with the

---

[5]Mass transfer on to a more massive companion results in a widening of the orbit and a lower mass-transfer rate compared to the case when the companion is the less massive star.

V17 rate, it seems as if stable mass-transfer leads to more Type IIb SNe than Type Ib SNe but we do not yet have a definitive statement. A statistical analysis is needed to compare binary evolution models with the overall rates of different types of CCSNe (Smith et al. 2011; Graur et al. 2017).

The absence of known analogues to our suggested hydrogen-poor giant Type IIb SNe progenitors is puzzling. At high temperatures, such as most of our NL00 models, the primary stars can remain hidden by their companions because most of the luminosity is output in the far-ultraviolet (Götberg et al. 2018). Our V17 models with lower mass-loss rates should at some point in their evolution be significantly cooler and more visible. So we would expect to see more such stars in the Milky Way or the Local Group. One relevant example is the helium giant υ Sagittarii (Schoenberner & Drilling 1983; Dudley & Jeffery 1990; Kipper & Klochkova 2012).

In another set of models we changed the mixing assumptions described in Section 2.4 and the Schwarzschild criterion and step overshooting were used. Several more models with the NL00 prescription in this set retained a hydrogen envelope but these were still the minority. The V17 models were unaffected. This is a consequence of the dependence on the helium fraction in the NL00 prescription. This does not exist in the V17 prescription. While the qualitative results are not affected by the mixing assumptions, quantitatively the rates of Type Ib and Type IIb SNe can change, indicating another sensitivity to an uncertain process which affects stellar modelling.

Our study has further implications for a number of issues.

(i) Sravan, Marchant & Kalogera (2018) find it difficult to account for the rate of Type IIb SNe at solar metallicity. They note that lower mass-loss rates would alleviate the situation. Our findings strongly support this idea, though a rigorous statistical analysis is warranted, specifically to address the impact on Type Ib rates and to compare with observed rates.

(ii) Helium giant stars with final masses in the range $2 < M/M_\odot < 4$ have been suggested as possible progenitors of rapidly fading supernovae (Kleiser, Fuller & Kasen 2018). Our stellar models share many similarities with those of Kleiser et al. (2018) even when the stars retain some hydrogen. These might also be relevant for rapidly fading supernovae. Wind mass-loss in helium stars is similarly important for electron-capture SNe in binary systems (Tauris et al. 2015; Moriya & Eldridge 2016).

(iii) The implications for the ionizing radiation provided by massive stars which have lost their envelopes by RLOF need to be assessed (Stanway, Eldridge & Becker 2016; Götberg, de Mink & Groh 2017; Xiao, Stanway & Eldridge 2018). Our models with the V17 mass-loss rate reach hot UV-producing regions in the Hertzsprung–Russell diagram during part of their evolution (see Fig. 1) but do not get as hot as the models with the NL00 mass-loss rate.

We end by reiterating that the main point of this study is to illustrate the sensitivity of evolutionary models for CCSN progenitors and the need for a sound theoretical understanding of stellar winds.

REFERENCES

Arcavi I. et al., 2017, ApJ, 837, L2
Bestenlehner J. M. et al., 2014, A&A, 570, A38
Claeys J. S. W., de Mink S. E., Pols O. R., Eldridge J. J., Baes M., 2011, A&A, 528, A131
de Jager C., Nieuwenhuijzen H., van der Hucht K. A., 1988, A&AS, 72, 259
Dessart L., Hillier D. J., Livne E., Yoon S.-C., Woosley S., Waldman R., Langer N., 2011, MNRAS, 414, 2985
Dudley R. E., Jeffery C. S., 1990, MNRAS, 247, 400
Eldridge J. J., Fraser M., Smartt S. J., Maund J. R., Crockett R. M., 2011, MNRAS, 414, 2985
Eldridge J. J., Stanway E. R., Xiao L., McClelland L. A. S., Taylor G., Ng M., Freis S. M. L., Bray J. C., 2017, PASA, 34, 58
Filippenko A. V., 1997, ARA&A, 35, 309
Folatelli G., Bersten M. C., Kuncarayakti H., Benvenuto O. G., Maeda K., Nomoto K., 2015, ApJ, 811, 147
Götberg Y., de Mink S. E., Groh J. H., 2017, A&A, 608, A11
Götberg Y., de Mink S. E., Groh J. H., Kupfer T., Crowther P. A., Zapartas E., Renzo M., 2018, A&A, 615, A78
Graur O., Bianco F. B., Modjaz M., Shivvers I., Filippenko A. V., Li W., Smith N., 2017, ApJ, 837, 121
Groh J. H., Oliveira A. S., Steiner J. E., 2008, A&A, 485, 245
Habets G. M. H. J., 1986, A&A, 167, 61
Henyey L., Vardya M. S., Bodenheimer P., 1965, ApJ, 142, 841
Herwig F., 2000, A&A, 360, 952
Kerzendorf W. E. et al., 2019, A&A, 623, A34
Kilpatrick C. D. et al., 2017, MNRAS, 465, 4650
Kippenhahn R., Ruschenplatt G., Thomas H.-C., 1980, A&A, 91, 175
Kipper T., Klochkova V. G., 2012, Balt. Astron., 21, 219
Kleiser I., Fuller J., Kasen D., 2018, MNRAS, 481, L141
Kochanek C. S., 2018, MNRAS, 473, 1633
Kolb U., Ritter H., 1990, A&A, 236, 385
Kotak R., Vink J. S., 2006, A&A, 460, L5
Langer N., Fricke K. J., Sugimoto D., 1983, A&A, 126, 207
Maund J. R., Smartt S. J., Kudritzki R. P., Podsiadlowski P., Gilmore G. F., 2004, Nature, 427, 129
Maund J. R. et al., 2011, ApJ, 739, L37
McClelland L. A. S., Eldridge J. J., 2016, MNRAS, 459, 1505
Moriya T. J., Eldridge J. J., 2016, MNRAS, 461, 2155
Nomoto K., Suzuki T., Shigeyama T., Kumagaim S., Yamaoka H., Saio H., 1993, Nature, 364, 507
Nugis T., Lamers H. J. G. L. M., 2000, A&A, 360, 227
Packet W., 1981, A&A, 102, 17
Paxton B. et al., 2013, ApJS, 208, 4
Paxton B. et al., 2015, ApJS, 220, 15
Paxton B. et al., 2018, ApJS, 234, 34
Paxton B., Bildsten L., Dotter A., Herwig F., Lesaffre P., Timmes F., 2011, ApJS, 192, 3
Podsiadlowski P., Hsu J. J. L., Joss P. C., Ross R. R., 1993, Nature, 364, 509
Puls J., Vink J. S., Najarro F., 2008, A&AR, 16, 209
Schoenberner D., Drilling J. S., 1983, ApJ, 268, 225
Smith N., Li W., Filippenko A. V., Chornock R., 2011, MNRAS, 412, 1522
Soker N., 2017, MNRAS, 470, L102
Sravan N., Marchant P., Kalogera V., 2018, preprint (arXiv:1808.07580)
Stanway E. R., Eldridge J. J., Becker G. D., 2016, MNRAS, 456, 485
Sukhbold T., Woosley S. E., Heger A., 2018, ApJ, 860, 93
Tartaglia L. et al., 2017, ApJ, 836, L12
Tauris T. M., Langer N., Podsiadlowski P., 2015, MNRAS, 451, 2123
Van Dyk S. D. et al., 2014, AJ, 147, 37
Vink J. S., 2017, A&A, 670, L8
Vink J. S., de Koter A., Lamers H. J. G. L. M., 1999, A&A, 350, 181
Vink J. S., de Koter A., Lamers H. J. G. L. M., 2001, A&A, 369, 574
Vink J. S., Muijres L. E., Anthonisse B., de Koter A., Gräfener G., Langer N., 2011, A&A, 531, A132
Woosley S. E., Heger A., Weaver T. A., 2002, Rev. Mod. Phys., 74, 1015
Xiao L., Stanway E. R., Eldridge J. J., 2018, MNRAS, 477, 904
Yoon S.-C., 2015, Publ. Astron. Soc. Aust., 32, e015

Yoon S.-C., 2017, MNRAS, 470, 3970
Yoon S.-C., Gräfener G., Vink J. S., Kozyreva A., Izzard R. G., 2012, A&A, 544, L11
Yoon S.-C., Dessart L., Clocchiatti A., 2017, ApJ, 840, 10

APPENDIX A: CODE IMPLEMENTATION

Here we list some specific details of the MESA implementation.

The wind mass-loss rate was calculated with the `other_wind` hook in the MESA `run_star_extras.f` file. An input parameter (`x_character_ctrl`) was used to distinguish between the NL00 and V17 schemes. Except for the hot hydrogen-deficient phase of models which employed the V17 prescription, the mass-loss rate was similar to the Dutch scheme of MESA.

The mass-transfer efficiency was limited according to two criteria. The first is equation (3) which gives

$$\beta_{\rm th} = \frac{1}{\tau_{\rm th}} \frac{M}{\dot{M}_{\rm tr}}. \tag{A1}$$

The second criterion is related to the radius of the accretor compared to its Roche lobe radius. This gives

$$\beta_{\rm L} = \begin{cases} 1, & R_2 \leq 0.99 R_{\rm L,2}, \\ f_3\left(R_2/R_{\rm L,2}\right), & 0.99 R_{\rm L,2} < R_2 < R_{\rm L,2}, \\ 0, & R_2 \geq R_{\rm L,2}, \end{cases} \tag{A2}$$

with

$$f_3(x) = 10^6 \left(2x^3 - 5.97x^2 + 5.94x - 1.97\right). \tag{A3}$$

The two criteria are combined as

$$\beta_{\rm max} = \min\left(\beta_{\rm th}, \beta_{\rm L}, 0.9\right). \tag{A4}$$

The enforcement of equation (A4) was made by the function `extras_binary_check_model` in the MESA `run_binary_extras.f` file. Whenever β used for a time step deviates from that calculated by equation (A4) with given M, L, R, R_2 and $R_{\rm L,2}$ at the end of the time step by more than $\Delta\beta$ (chosen as $\Delta\beta = 0.001$) `extras_binary_check_model` tells the code to rerun the time-step with a different β, chosen in an informed manner. This is iterated until convergence in a similar way to the implicit method of mass transfer described by Paxton et al. (2015). We note that the mass-transfer rate itself $\dot{M}_{\rm tr}$ is computed explicitly from the stellar parameters at the beginning of the time-step.

In addition to the mixing described in Section 2.4, the outermost part of the accretor had enhanced mixing, implemented with the `other_D_mix` hook. The part for enhanced mixing was chosen as the region defined by $0.99 < m/M_2 < 1$, where m is the mass coordinate within the accretor and M_2 is the total mass of the accretor. In this region the mixing coefficient is set to $D_{\rm mix,out} = 10^{20}\,{\rm cm}^2\,{\rm s}^{-1}$ but only if the star is gaining mass. This mixing enhancement is added because the accretion of material with a composition significantly different from the surface composition of the accretor causes abrupt changes in the surface opacity and radius, and related quantities. The enhanced mixing ensures a smooth evolution of the secondary during accretion of helium-rich material. Because our focus is on the properties of the primary, which are anyway rather insensitive to the details of the secondary, this modification is of minor importance.

APPENDIX B: STELLAR MODELS

The initial parameters we used give a total of 198 different combinations. Of these 93 never reached a point in their evolution

Table B1. Initial parameters for which convergence problems arise after reaching $X_{\rm s} < 0.4$.

M_1/ $M_\odot$	M_2/ $M_\odot$	$P_{\rm i}$/ d	Mass-loss recipe –
12	5	5	NL00
16	10	33	NL00
22	8	10	V17

Table B2. Initial parameters for which the evolution headed towards common envelope evolution after reaching $X_{\rm s} < 0.4$, regardless of the mass-loss recipe employed.

M_1/ $M_\odot$	M_2/ $M_\odot$	$P_{\rm i}$/ d
12	5	1219
14	5	669
14	5	1219
16	6	669
16	6	1219
16	6	2223
19	7	1219

at which $X_{\rm s} < 0.4$ and are not discussed or presented (except for the $M_1 = 12\,{\rm M_\odot}$, $M_2 = 10\,{\rm M_\odot}$, $P_{\rm i} = 367$ d track shown in Fig. 1). The remaining 105 combinations of initial parameters become 210 separate evolutionary tracks because different mass-loss recipes are used once $X_{\rm s} < 0.4$. Of these 3 (listed in Table B1) have convergence problems and 14 (listed in Table B2) head towards common envelope evolution. The properties of interest for the remaining 193 binary systems modelled are listed in Tables B3–B8, where $f_{\rm L} = (R - R_{\rm L,1})/R_{\rm L,1}$, where $R_{\rm L,1}$ is the Roche lobe radius of the primary. The mass-loss rate given in the last column is the sum of the wind mass-loss rate and mass-transfer rate by RLOF. The other properties listed in the tables have been defined earlier. These 193 models, all of which reached central carbon depletion, are presented and discussed throughout the paper.

The evolution of the primary as a single star after core carbon depletion was continued until iron core collapse for 95 models. The remaining time until core collapse was found to be $\Delta t \lesssim 30$ yr. For models with $M \lesssim 7\,{\rm M_\odot}$ at the end of the binary evolution the remaining time closely follows the relation

$$\log_{10}\left(\Delta t/{\rm yr}\right) \simeq 2.4985 - 1.8934 \log_{10}\left({\rm M/M_\odot}\right), \tag{B1}$$

where the mass M at core carbon depletion is approximately the helium core mass,[6] because the hydrogen envelope is either of very low mass or non-existent. Models with $M \gtrsim 7\,{\rm M_\odot}$ do not follow equation (B1) and have much shorter time-scales, with $\Delta t < 1$ yr for the highest masses. Models with $M \lesssim 3.3\,{\rm M_\odot}$ did not reach core collapse so we extrapolate with equation (B1) for the model with the lowest mass to a remaining time of $\Delta t \approx 48$ yr. The range we find for Δt is similar to the time-scales for neon and oxygen burning in the core given by table 1 of Woosley et al. (2002) with an additional delay time of several years between core carbon depletion and neon ignition. This shows that we can expect negligible changes between the end of our binary simulations and terminal iron core collapse.

---

[6] The helium core mass is tightly correlated to the carbon–oxygen core mass.

Table B3. Initial parameters and final properties for stellar evolution calculations with $0.9 > q > 0.8$ with the V17 prescription.

$M_1/$ $M_\odot$	$M_2/$ $M_\odot$	$P_i/$ d	$M_H/$ $M_\odot$	$M/$ $M_\odot$	$R/$ $R_\odot$	$T_{eff}/$ K	$L/$ $L_\odot$	M_v	X_s	Y_s	f_L	$\log_{10}\left(|\dot{M}|/M_\odot\,\mathrm{yr}^{-1}\right)$
12	10	5	0.0075	3.09	35.49	14 538	50 539	−6.2	0.22	0.76	0.033	−5.29
12	10	10	0.0101	3.14	54.81	11 760	51 616	−6.3	0.23	0.75	0.023	−5.3
12	10	18	0.012	3.16	80.3	9744	52 219	−6.3	0.24	0.74	0.019	−5.28
12	10	33	0.0146	3.19	118.9	8029	52 786	−6.3	0.25	0.73	0.008	−5.29
12	10	60	0.0183	3.22	175.53	6627	53 373	−6.3	0.26	0.72	−0.013	−5.29
12	10	110	0.0272	3.29	253.89	5539	54 531	−6.4	0.27	0.71	−0.038	−5.4
12	10	201	0.0359	3.37	291.96	5216	56 679	−6.4	0.31	0.67	−0.224	−5.98
14	12	5	0.0248	4.05	33.45	16 671	77 654	−6.4	0.24	0.74	0.064	−5.05
14	12	10	0.029	4.11	43.54	14 686	79 225	−6.7	0.25	0.73	0.051	−6.64
14	12	18	0.0318	4.13	50.43	13 676	79 932	−6.8	0.26	0.72	0.007	−6.64
14	12	33	0.0331	4.16	58.31	12 741	80 497	−6.8	0.27	0.72	−0.209	−6.64
14	12	60	0.0345	4.18	68.6	11 771	81 164	−6.8	0.27	0.71	−0.37	−6.63
14	12	110	0.0362	4.21	89.65	10 317	81 798	−6.8	0.28	0.7	−0.487	−6.29
14	12	201	0.0413	4.28	162.01	7712	83 412	−6.8	0.3	0.68	−0.474	−5.97
14	12	367	0.0421	4.3	174.53	7446	84 135	−6.8	0.31	0.68	−0.603	−5.94
16	14	5	0.0312	4.96	12.62	29 448	107 581	−5.4	0.25	0.73	−0.517	−6.46
16	14	10	0.0352	5.03	16.83	25 605	109 411	−5.8	0.27	0.71	−0.572	−6.45
16	14	110	0.044	5.15	36.52	17 516	112 776	−6.7	0.29	0.69	−0.802	−6.44
16	14	201	0.0472	5.2	51.9	14 729	113 919	−7.1	0.3	0.68	−0.82	−6.43
16	14	367	0.0467	5.19	49.38	15 098	113 841	−7	0.3	0.68	−0.882	−6.43
16	14	669	0.0516	5.27	88.74	11 323	116 305	−7.2	0.31	0.67	−0.848	−6.42
19	16	5	0.0143	5.86	3.04	64 430	143 389	−3.9	0.14	0.84	−0.89	−6.29
19	16	10	0.0256	5.73	6.63	43 133	136 858	−4.8	0.21	0.77	−0.858	−6.32
19	16	18	0.026	5.95	9.19	37 194	145 246	−5.2	0.36	0.63	−0.866	−6.28
19	16	33	0.0181	5.95	3.39	61 363	146 135	−4.1	0.15	0.83	−0.965	−6.28
22	19	5	0.013	7.23	2.16	82 848	197 679	−3.7	0.13	0.85	−0.925	−6.11
22	19	10	0.0304	7.07	4.72	55 393	188 335	−4.6	0.21	0.77	−0.902	−6.13
25	22	5	0.0124	8.69	1.78	97 740	258 873	−3.6	0.13	0.85	−0.94	−5.95

Table B4. Initial parameters and final properties for stellar evolution calculations with $0.9 > q > 0.8$ with the NL00 prescription.

$M_1/$ $M_\odot$	$M_2/$ $M_\odot$	$P_i/$ d	$M_H/$ $M_\odot$	$M/$ $M_\odot$	$R/$ $R_\odot$	$T_{eff}/$ K	$L/$ $L_\odot$	M_v	X_s	Y_s	f_L	$\log_{10}\left(|\dot{M}|/M_\odot\,\mathrm{yr}^{-1}\right)$
12	10	5	0	2.79	8.76	28 256	43 960	−4.6	0	0.98	−0.461	−5.89
12	10	10	0	2.82	8.19	29 378	44 898	−4.5	0	0.98	−0.721	−5.88
12	10	18	0	2.85	7.67	30 466	45 497	−4.4	0	0.98	−0.836	−5.87
12	10	33	0	2.87	7.38	31 150	46 053	−4.4	0	0.98	−0.9	−5.87
12	10	60	0	2.89	7.02	32 026	46 644	−4.3	0	0.98	−0.94	−5.86
12	10	110	0	2.94	6.48	33 569	47 964	−4.3	0	0.98	−0.966	−5.84
12	10	201	0	3.03	5.77	36 062	50 593	−4.1	0	0.98	−0.981	−5.81
14	12	5	0	3.48	3.81	47 440	66 065	−3.8	0	0.98	−0.865	−5.66
14	12	10	0	3.53	3.66	48 683	67 612	−3.8	0	0.98	−0.915	−5.65
14	12	18	0	3.55	3.58	49 344	68 431	−3.8	0	0.98	−0.944	−5.64
14	12	33	0	3.58	3.52	49 954	69 268	−3.7	0	0.98	−0.964	−5.64
14	12	60	0	3.61	3.44	50 714	70 147	−3.7	0	0.98	−0.977	−5.63
14	12	110	0	3.64	3.34	51 682	71 357	−3.7	0	0.98	−0.985	−5.62
14	12	201	0	3.73	3.12	53 966	74 097	−3.6	0	0.98	−0.991	−5.6
14	12	367	0.0375	4.29	132.02	8562	84 167	−6.8	0.3	0.68	−0.688	−6.04
16	14	5	0	4.15	2.22	66 826	88 172	−3.3	0	0.98	−0.921	−5.5
16	14	10	0	4.2	2.14	68 460	89 973	−3.3	0	0.98	−0.952	−5.49
16	14	110	0	4.35	1.96	72 360	94 599	−3.2	0	0.98	−0.991	−5.46
16	14	201	0	4.41	1.9	73 946	96 637	−3.2	0	0.98	−0.994	−5.45
16	14	367	0	4.57	1.77	77 640	102 082	−3.1	0	0.98	−0.996	−5.42
16	14	669	0.0308	5.2	19.64	24 117	117 223	−6	0.3	0.68	−0.969	−5.61
19	16	5	0	4.68	1.53	84 205	106 060	−3	0	0.98	−0.947	−5.4
19	16	10	0	4.6	1.62	81 333	103 510	−3.1	0	0.98	−0.966	−5.41
19	16	18	0.0249	5.94	6.01	45 968	145 061	−4.7	0.23	0.75	−0.91	−5.42
19	16	33	0.0039	5.83	2.04	78 963	144 673	−3.5	0.11	0.87	−0.98	−5.31
22	19	5	0	5.53	1.04	108 497	135 133	−2.7	0	0.98	−0.963	−5.26
22	19	10	0.0102	6.95	2.27	79 799	187 614	−3.7	0.16	0.82	−0.953	−5.21
25	22	5	0	6.38	0.86	125 125	163 105	−2.6	0	0.98	−0.97	−5.16

Table B5. Initial parameters and final properties for stellar evolution calculations with $0.7 > q > 0.6$ with the V17 prescription.

$M_1/$ $M_\odot$	$M_2/$ $M_\odot$	$P_i/$ d	$M_H/$ $M_\odot$	$M/$ $M_\odot$	$R/$ $R_\odot$	$T_{eff}/$ K	$L/$ $L_\odot$	M_v	X_s	Y_s	f_L	$\log_{10}\left(|\dot{M}|/M_\odot\,\mathrm{yr}^{-1}\right)$
12	8	5	0.0063	3.07	29.17	15 996	50 046	−6	0.21	0.77	0.042	−5.37
12	8	10	0.0089	3.12	44.17	13 080	51 312	−6.3	0.23	0.75	0.025	−5.29
12	8	18	0.011	3.15	64.94	10 824	51 995	−6.3	0.24	0.74	0.022	−5.28
12	8	33	0.0129	3.17	95.67	8940	52 519	−6.3	0.24	0.74	0.017	−5.29
12	8	60	0.0156	3.2	135.91	7518	53 008	−6.3	0.25	0.73	0.002	−5.29
12	8	110	0.0198	3.23	194.22	6306	53 604	−6.3	0.26	0.72	−0.018	−5.28
12	8	201	0.0312	3.32	270.61	5383	55 240	−6.4	0.28	0.7	−0.095	−6.02
12	8	367	0.0412	3.4	311.49	5067	57 475	−6.4	0.35	0.63	−0.275	−5.95
14	9	5	0.0222	4.02	25.92	18 863	76 431	−6.1	0.24	0.75	0.056	−4.74
14	9	10	0.0265	4.09	38.47	15 600	78 757	−6.6	0.25	0.73	0.066	−5.71
14	9	18	0.0301	4.12	46.9	14 165	79 557	−6.8	0.26	0.72	0.035	−6.64
14	9	33	0.0323	4.14	53.61	13 274	80 161	−6.8	0.26	0.72	−0.052	−6.64
14	9	60	0.0335	4.16	60.77	12 487	80 667	−6.8	0.27	0.71	−0.235	−6.63
14	9	110	0.0347	4.19	71.2	11 555	81 191	−6.8	0.27	0.71	−0.393	−6.63
14	9	201	0.0368	4.22	99.71	9786	81 919	−6.8	0.28	0.7	−0.503	−6.16
14	9	367	0.0429	4.3	180.91	7308	83 853	−6.8	0.31	0.68	−0.469	−5.92
14	9	669	0.0405	4.3	162.31	7725	84 276	−6.8	0.31	0.67	−0.653	−5.96
16	10	5	0.0289	4.93	11.22	31 160	106 634	−5.3	0.24	0.74	−0.445	−6.47
16	10	10	0.033	5	14.13	27 901	108 698	−5.6	0.26	0.72	−0.52	−6.46
16	10	18	0.0364	5.05	18.12	24 708	109 964	−5.9	0.27	0.71	−0.571	−6.45
16	10	33	0.039	5.08	22.5	22 223	110 913	−6.1	0.28	0.7	−0.636	−6.45
16	10	60	0.0407	5.11	26.3	20 584	111 586	−6.3	0.28	0.7	−0.702	−6.44
16	10	110	0.0422	5.13	30.3	19 197	112 028	−6.5	0.29	0.69	−0.762	−6.44
16	10	201	0.0443	5.16	37.85	17 211	112 946	−6.7	0.29	0.69	−0.808	−6.44
16	10	367	0.0476	5.2	53.86	14 464	114 094	−7.1	0.3	0.68	−0.822	−6.43
16	10	669	0.0467	5.19	49.63	15 064	113 933	−7	0.3	0.68	−0.884	−6.43
16	10	1219	0.0512	5.26	83.3	11 682	116 073	−7.2	0.31	0.67	−0.853	−6.42
19	12	5	0.0132	5.81	2.92	65 627	141 914	−3.9	0.14	0.85	−0.867	−6.3
19	12	10	0.0262	5.71	6.9	42 240	136 163	−4.9	0.22	0.76	−0.805	−6.32
19	12	18	0.0262	5.91	8.47	38 644	143 652	−5.1	0.27	0.72	−0.837	−6.29
19	12	33	0.0182	5.95	3.41	61 164	146 172	−4.1	0.15	0.83	−0.956	−6.28
22	14	5	0.0116	7.16	2.06	84 502	194 813	−3.7	0.12	0.86	−0.906	−6.11
25	16	5	0.0107	8.59	1.68	100 070	255 079	−3.6	0.12	0.86	−0.928	−5.95
25	16	10	0.0454	7.99	44.33	18 860	223 347	−7.3	0.36	0.62	0.064	−4.26

Table B6. Initial parameters and final properties for stellar evolution calculations with $0.7 > q > 0.6$ with the NL00 prescription.

$M_1/$ $M_\odot$	$M_2/$ $M_\odot$	$P_i/$ d	$M_H/$ $M_\odot$	$M/$ $M_\odot$	$R/$ $R_\odot$	$T_{eff}/$ K	$L/$ $L_\odot$	M_v	X_s	Y_s	f_L	$\log_{10}\left(|\dot{M}|/M_\odot\,\mathrm{yr}^{-1}\right)$
12	8	5	0	2.78	9.04	27 760	43 600	− 4.6	0	0.98	− 0.271	− 5.9
12	8	10	0	2.82	8.19	29 338	44 645	− 4.5	0	0.98	− 0.633	− 5.88
12	8	18	0	2.84	7.87	30 037	45 269	− 4.4	0	0.98	− 0.79	− 5.87
12	8	33	0	2.86	7.46	30 937	45 794	− 4.4	0	0.98	− 0.871	− 5.87
12	8	60	0	2.87	7.26	31 434	46 276	− 4.4	0	0.98	− 0.918	− 5.86
12	8	110	0	2.9	6.92	32 310	46 885	− 4.3	0	0.98	− 0.949	− 5.86
12	8	201	0	2.96	6.22	34 406	48 739	− 4.2	0	0.98	− 0.973	− 5.83
12	8	367	0	3.09	5.5	37 212	52 128	− 4.1	0	0.98	− 0.985	− 5.8
14	9	5	0	3.46	3.88	46 912	65 369	− 3.8	0	0.98	− 0.811	− 5.67
14	9	10	0	3.51	3.71	48 225	67 032	− 3.8	0	0.98	− 0.889	− 5.66
14	9	18	0	3.54	3.62	49 005	68 019	− 3.8	0	0.98	− 0.927	− 5.65
14	9	33	0	3.56	3.55	49 627	68 769	− 3.7	0	0.98	− 0.95	− 5.64
14	9	60	0	3.59	3.49	50 196	69 465	− 3.7	0	0.98	− 0.967	− 5.64
14	9	110	0	3.61	3.42	50 873	70 328	− 3.7	0	0.98	− 0.979	− 5.63
14	9	201	0	3.65	3.3	52 032	71 724	− 3.7	0	0.98	− 0.987	− 5.62
14	9	367	0	3.75	3.06	54 620	74 853	− 3.6	0	0.98	− 0.992	− 5.59
14	9	669	0.0388	4.29	146.12	8142	84 287	− 6.8	0.3	0.68	− 0.686	− 6
16	10	5	0	4.12	2.26	66 065	87 253	− 3.3	0	0.98	− 0.891	− 5.51
16	10	10	0	4.18	2.17	67 754	89 157	− 3.3	0	0.98	− 0.934	− 5.5
16	10	18	0	4.22	2.11	68 918	90 444	− 3.3	0	0.98	− 0.957	− 5.49
16	10	60	0	4.28	2.04	70 528	92 343	− 3.3	0	0.98	− 0.981	− 5.48
16	10	110	0	4.31	1.99	71 583	93 566	− 3.2	0	0.98	− 0.988	− 5.47
16	10	201	0	4.35	1.95	72 509	94 751	− 3.2	0	0.98	− 0.992	− 5.46
16	10	367	0	4.42	1.89	74 204	96 958	− 3.2	0	0.98	− 0.995	− 5.45
16	10	669	0	4.59	1.75	78 080	102 815	− 3.1	0	0.98	− 0.996	− 5.42
16	10	1219	0.021	5.15	11.47	31 544	117 001	− 5.4	0.29	0.69	− 0.983	− 5.6
19	12	5	0	4.65	1.55	83 569	105 284	− 3	0	0.98	− 0.93	− 5.4
19	12	10	0	4.61	1.62	81 506	103 797	− 3	0	0.98	− 0.956	− 5.41
19	12	18	0	5.41	1.39	93 521	132 565	− 3	0	0.98	− 0.974	− 5.27
19	12	33	0.0009	5.78	1.63	88 240	144 636	− 3.2	0.05	0.93	− 0.979	− 5.26
22	14	5	0	5.49	1.05	107 880	134 159	− 2.7	0	0.98	− 0.95	− 5.27
25	16	5	0	6.32	0.89	122 343	160 372	− 2.6	0	0.98	− 0.959	− 5.17
25	16	10	0	6.89	0.97	122 289	190 807	− 2.8	0	0.98	− 0.975	− 5.07

Table B7. Initial parameters and final properties for stellar evolution calculations with $0.45 > q > 0.35$ with the V17 prescription.

$M_1/$ $M_\odot$	$M_2/$ $M_\odot$	$P_i/$ d	$M_H/$ $M_\odot$	$M/$ $M_\odot$	$R/$ $R_\odot$	$T_{eff}/$ K	$L/$ $L_\odot$	M_v	X_s	Y_s	f_L	$\log_{10}\left(|\dot{M}|/M_\odot\,\text{yr}^{-1}\right)$
12	5	5	0.0009	2.96	10.2	26 706	47 524	−4.8	0.13	0.85	0.043	−5.59
12	5	10	0.0034	3.03	16.56	21 141	49 217	−5.3	0.19	0.8	0.033	−5.61
12	5	18	0.0055	3.08	23.14	17 989	50 371	−5.7	0.21	0.77	0.041	−5.29
12	5	33	0.0077	3.11	35.44	14 596	51 231	−6.2	0.22	0.76	0.035	−5.31
12	5	60	0.01	3.14	52.09	12 079	51 891	−6.3	0.23	0.75	0.026	−5.29
12	5	110	0.0119	3.17	77.85	9903	52 372	−6.3	0.24	0.74	0.023	−5.34
12	5	201	0.0142	3.19	114.62	8180	52 840	−6.3	0.25	0.73	0.007	−5.28
12	5	367	0.0177	3.22	165.81	6816	53 327	−6.3	0.26	0.72	−0.009	−5.32
12	5	669	0.0247	3.27	239.51	5697	54 292	−6.4	0.27	0.71	−0.033	−5.3
14	5	5	0.0038	3.75	6.55	36 851	71 080	−4.5	0.16	0.82	0.06	−4.8
14	5	10	0.0108	3.88	10.16	29 861	73 693	−5	0.2	0.78	0.046	−4.62
14	5	18	0.016	3.96	14.97	24 727	75 280	−5.4	0.22	0.76	0.054	−4.6
14	5	33	0.0208	4.03	22.57	20 267	77 236	−5.9	0.24	0.74	0.052	−4.5
14	5	60	0.0247	4.08	34.08	16 526	77 834	−6.4	0.25	0.73	0.073	−4.68
14	5	110	0.0284	4.11	45.41	14 389	79 444	−6.8	0.26	0.73	0.057	−6.59
14	5	201	0.0318	4.14	51.86	13 490	80 032	−6.8	0.26	0.72	0.045	−6.64
14	5	367	0.0331	4.16	58	12 776	80 538	−6.8	0.27	0.72	−0.158	−6.64
16	6	5	0.0199	4.75	7.36	37 973	101 080	−4.8	0.19	0.79	0.096	−6
16	6	10	0.0244	4.86	8.82	34 967	104 471	−5	0.21	0.77	−0.157	−6.48
16	6	18	0.0275	4.92	10.39	32 367	106 411	−5.2	0.24	0.74	−0.327	−6.47
16	6	33	0.0312	4.97	12.56	29 539	107 938	−5.4	0.25	0.73	−0.422	−6.46
16	6	60	0.0344	5.02	15.55	26 623	109 183	−5.7	0.26	0.72	−0.495	−6.46
16	6	110	0.0374	5.06	19.64	23 752	110 251	−6	0.27	0.71	−0.561	−6.45
16	6	201	0.0395	5.09	23.36	21 818	111 105	−6.2	0.28	0.7	−0.638	−6.45
16	6	367	0.0411	5.11	27.61	20 096	111 701	−6.4	0.28	0.7	−0.708	−6.44
19	7	5	0.0114	5.74	2.73	67 581	139 282	−3.8	0.12	0.86	−0.671	−6.31
19	7	10	0.0286	5.85	9.1	37 113	141 268	−5.2	0.25	0.73	−0.172	−6.3
19	7	33	0.0161	5.91	3.17	63 351	144 980	−4	0.15	0.84	−0.873	−6.29
19	7	110	0.0191	5.94	3.61	59 453	145 901	−4.1	0.16	0.82	−0.933	−6.28
19	7	201	0.0192	5.95	3.63	59 294	146 165	−4.2	0.16	0.82	−0.956	−6.28
19	7	367	0.0202	5.97	3.69	58 867	146 630	−4.2	0.16	0.82	−0.97	−6.28
19	7	669	0.0211	5.99	3.79	58 120	147 110	−4.2	0.16	0.82	−0.979	−6.28
22	8	5	0.005	6.7	1.68	91 358	177 100	−3.4	0.06	0.92	−0.807	−6.17
25	9	5	0.005	7.99	1.43	105 960	230 583	−3.3	0.06	0.92	−0.842	−6.01
25	9	10	0.0249	7.7	17.34	29 929	216 801	−6.2	0.38	0.6	0.05	−5.06

Table B8. Initial parameters and final properties for stellar evolution calculations with $0.45 > q > 0.35$ with the NL00 prescription.

$M_1/$ $M_\odot$	$M_2/$ $M_\odot$	$P_i/$ d	$M_H/$ $M_\odot$	$M/$ $M_\odot$	$R/$ $R_\odot$	$T_{eff}/$ K	$L/$ $L_\odot$	M_v	X_s	Y_s	f_L	$\log_{10}\left(|\dot{M}|/M_\odot\,\mathrm{yr}^{-1}\right)$
12	5	10	0	2.75	9.5	26 980	42 948	−4.6	0	0.98	0.017	−5.9
12	5	18	0	2.79	8.82	28 148	43 849	−4.6	0	0.98	−0.215	−5.89
12	5	33	0	2.81	8.32	29 104	44 605	−4.5	0	0.98	−0.536	−5.88
12	5	60	0	2.83	7.77	30 217	45 168	−4.4	0	0.98	−0.744	−5.88
12	5	110	0	2.85	7.54	30 752	45 650	−4.4	0	0.98	−0.843	−5.87
12	5	201	0	2.87	7.42	31 060	46 092	−4.4	0	0.98	−0.902	−5.86
12	5	367	0	2.89	7.08	31 895	46 601	−4.3	0	0.98	−0.939	−5.86
12	5	669	0	2.92	6.62	33 173	47 653	−4.3	0	0.98	−0.964	−5.85
14	5	5	0	3.31	4.49	42 672	60 004	−3.9	0	0.98	−0.184	−5.72
14	5	10	0	3.38	4.16	44 796	62 677	−3.9	0	0.98	−0.509	−5.69
14	5	18	0	3.44	3.97	46 154	64 397	−3.8	0	0.98	−0.69	−5.68
14	5	33	0	3.48	3.82	47 306	65 819	−3.8	0	0.98	−0.802	−5.67
14	5	60	0	3.51	3.72	48 180	66 928	−3.8	0	0.98	−0.871	−5.66
14	5	110	0	3.54	3.63	48 939	67 886	−3.8	0	0.98	−0.915	−5.65
14	5	201	0	3.56	3.57	49 479	68 571	−3.7	0	0.98	−0.943	−5.64
14	5	367	0	3.58	3.51	50 005	69 229	−3.7	0	0.98	−0.963	−5.64
16	6	5	0	3.98	2.5	61 895	82 629	−3.4	0	0.98	−0.636	−5.54
16	6	10	0	4.06	2.35	64 433	85 341	−3.4	0	0.98	−0.786	−5.52
16	6	18	0	4.12	2.26	65 965	87 024	−3.3	0	0.98	−0.862	−5.51
16	6	33	0	4.16	2.19	67 284	88 477	−3.3	0	0.98	−0.911	−5.5
16	6	60	0	4.2	2.14	68 325	89 671	−3.3	0	0.98	−0.941	−5.49
16	6	110	0	4.23	2.09	69 301	90 788	−3.3	0	0.98	−0.962	−5.49
16	6	201	0	4.26	2.06	70 045	91 679	−3.3	0	0.98	−0.975	−5.48
16	6	367	0	4.28	2.03	70 782	92 554	−3.3	0	0.98	−0.983	−5.47
19	7	5	0	4.64	1.56	83 159	104 662	−3	0	0.98	−0.822	−5.41
19	7	10	0	4.79	1.47	86 849	110 022	−3	0	0.98	−0.873	−5.38
19	7	33	0	5.55	1.4	93 983	137 913	−3	0	0.98	−0.941	−5.25
19	7	110	0	5.54	1.39	94 400	137 558	−3	0	0.98	−0.976	−5.25
19	7	201	0	5.55	1.39	94 472	138 110	−3	0	0.98	−0.984	−5.25
19	7	367	0	5.74	1.44	93 589	143 815	−3.1	0	0.98	−0.988	−5.23
19	7	669	0.0098	5.9	2.75	68 166	146 545	−3.8	0.15	0.83	−0.985	−5.34
22	8	5	0	5.17	1.18	99 642	123 196	−2.8	0	0.98	−0.868	−5.31
22	8	10	0	5.57	1.22	100 897	138 060	−2.9	0	0.98	−0.903	−5.25
25	9	5	0	5.94	0.96	115 772	147 516	−2.6	0	0.98	−0.9	−5.21
25	9	10	0.0248	7.7	17.22	30 035	216 838	−6.2	0.38	0.6	0.044	−5.02

This paper has been typeset from a TEX/LATEX file prepared by the author.